ARTICLES
https://doi.org/10.1038/s41477-018-0334-3
nature plants

# Identification of vacuolar phosphate efflux transporters in land plants

Lei Xu[1,7], Hongyu Zhao[1,7], Renjing Wan[2,7], Yu Liu[3], Zhuang Xu[2], Wang Tian[4], Wenyuan Ruan[1], Fang Wang[5], Minjuan Deng[5], Junmin Wang[5], Liam Dolan[6], Sheng Luan[4], Shaowu Xue[2*] and Keke Yi[1*]

**Inorganic phosphate (Pi) is an essential component of all life forms. Land plants acquire Pi from the soil through roots and associated symbioses, and it is then transported throughout the plant. When sufficient, excess Pi is stored in vacuoles for remobilization following Pi deficiency. Although Pi release from the vacuoles to the cytoplasm serves as a critical mechanism for plants to adapt to low-Pi stress, the transporters responsible for vacuolar Pi efflux have not been identified. Here, we identified a pair of *Oryza sativa* vacuolar Pi efflux transporters (OsVPE1 and OsVPE2) that were more abundant in plants grown under Pi-deficient conditions. These OsVPE proteins can transport Pi into yeast cells and *Xenopus laevis* oocytes. Vacuolar Pi content was higher in the loss-of-function *Osvpe1 Osvpe2* double mutant than in wild type, particularly under low-Pi stress. Overexpression of either *OsVPE1* or *OsVPE2* in transgenic plants reduced vacuolar Pi content, consistent with a role in vacuolar Pi efflux. We demonstrate that these VPE proteins evolved from an ancient plasma membrane glycerol-3-phosphate transporter protein. Together, these data indicate that this transporter was recruited to the vacuolar membrane to catalyse Pi efflux during the course of land plant evolution.**

Phosphorus is an essential element for plant growth and is taken up by plant roots as Pi. The amount of Pi in the soil that is available to the plant is often limiting for growth, because Pi forms insoluble precipitates with many metal cations and avidly binds to some plate silicates. Consequently, nearly 70% of global arable land suffers from Pi deficiency and this compromises plant growth and crop yields. Plants have evolved different strategies to adapt to changes in Pi availability. These include modulating the morphology of their roots, increasing their capacity to take up Pi at the plasma membrane and the capacity to mobilize Pi from intracellular stores, each of which facilitates plant adaptation to distinct soil microenvironments[1–3].

Pi transporters are located in cell membranes and catalyse the transport of Pi from one compartment to another. Pi is absorbed by plant roots via both low-affinity and high-affinity Pi transporters[4]. In angiosperms, the *Pht1* gene family encode Pi transporters that transport Pi across the plasma membrane of root cells located at the root–soil interface. The *Pht2*, *Pht3* and *Pht4* gene families encode proteins that transport Pi between the cytoplasm and different subcellular compartments[5–7]. Vacuoles are the major intracellular stores for excess Pi. This vacuolar reservoir is used to buffer Pi changes in the cytoplasm in response to changes in metabolic demand and availability of Pi in the soil. The vacuolar Pi/total Pi ratio can vary from 0 to 80%[8]. This ratio is low when the external Pi availability is insufficient and the vacuolar Pi store is remobilized to the cellular compartments where it is required, and the ratio is high when there is sufficient Pi supply. Recent studies have identified vacuolar Pi transporters (VPTs; also named Pi transporter type 5 (PHT5) family) with both the SYG1/PHO81/XPR1 (SPX) domain and the major facilitator superfamily (MFS) domain as vacuolar Pi transporters that sequester Pi into the vacuolar lumen in *Arabidopsis*[9,10]. Although the rice homologue SPX-MFS3 has been reported to be a vacuolar Pi efflux transporter in rice[11], our results here showed that it is a vacuolar Pi influx transporter, similar to its *Arabidopsis* homologues. Consequently, the transport proteins responsible for vacuolar Pi efflux remain unknown.

Glycerol-3-phosphate (G3P) serves as a carbon and energy source in *Escherichia coli* and is a precursor for phospholipid biosynthesis[12]. G3P uptake is facilitated by the inner membrane G3P transporter (GlpT), which belongs to the MFS family of proteins[13]. GlpT is an antiporter that facilitates G3P uptake into the cytoplasm and Pi into the periplasm and is energetically driven by a Pi gradient. The structure of GlpT in *E. coli* indicates that GlpT operates via a single binding site and an alternating access mechanism through a rocker-switch type of movement[13]. There are five GlpT homologues in *Arabidopsis*, and their expression increases under low-Pi conditions, suggesting a potential connection to Pi homeostasis[14]. AtG3Pp4 is located in plastids and is involved in the accumulation of storage lipids in late embryogenesis[15]. To date, however, there is no report showing an involvement of plant GlpT proteins in plant Pi homeostasis.

Here, we report the discovery of vacuolar GlpT proteins from rice that function in Pi homeostasis by facilitating vacuolar Pi efflux. We carried out a quantitative proteomic analysis of the vacuolar membrane proteins and identified of a pair of vacuolar GlpT proteins (OsVPE1 and OsVPE2) whose abundance increased in rice roots grown in Pi-starvation conditions. Heterologous expression of either OsVPE1 or OsVPE2 in yeast and oocytes demonstrated that they directly transport Pi. We further show that the OsVPE proteins are essential for vacuolar Pi efflux in rice under both Pi-replete and -deficient conditions. OsVPE1 and OsVPE2 are members of a monophyletic group of proteins (VPE) in angiosperms. The

[1]Key Laboratory of Plant Nutrition and Fertilizers, Ministry of Agriculture, Institute of Agricultural Resources and Regional Planning, Chinese Academy of Agricultural Sciences, Beijing, China. [2]College of Life Science and Technology, Huazhong Agricultural University, Wuhan, China. [3]College of Life Sciences, Zhejiang University, Hangzhou, China. [4]Department of Plant and Microbial Biology, University of California, Berkeley, CA, USA. [5]Zhejiang Academy of Agricultural Sciences, Hangzhou, China. [6]Department of Plant Sciences, University of Oxford, Oxford, UK. [7]These authors contributed equally: Lei Xu, Hongyu Zhao, Renjing Wan. *e-mail: xues@mail.hzau.edu.cn; yikeke@gmail.com

angiosperm VPE proteins and the GlpT proteins from early diverging land plants reside on the vacuolar membrane. Our results indicate that an ancestral plasma membrane GlpT was recruited to the vacuolar membrane during the course of land plant evolution, and it functions as a vacuolar Pi efflux transporter crucial for celluar Pi homeostasis.

## Results

**A pair of Pi starvation-induced VPE proteins are located on the vacuolar membrane in rice.** To identify vacuolar membrane proteins involved in Pi efflux under Pi-deficient stress in rice, we conducted an iTRAQ (isobaric tags for relative and absolute quantitation) analysis of total vacuolar membrane protein isolated from rice roots grown either in the absence of Pi or under replete Pi. In the assay, we identified the OsSPX-MFS3 protein, which was reported as a vacuolar Pi efflux transporter in rice[11]. However, the protein levels of it were reduced under Pi-deficient stress (Supplementary Fig. 1). The vacuolar Pi contents of the *OsSPX-MFS3* overexpressing lines and loss-of-function mutants measured by NMR spectroscopy were significantly higher and lower, respectivley, than that of wild type plants (Supplementary Fig. 2). This indicates that OsSPX-MFS3 is a vacuolar Pi influx transporter and that the vacuolar Pi efflux transporter in plants is still unknown.

From the iTRAQ analysis, two proteins (encoded by the genes *Os04G46880* and *Os08G06010*) were identified as inducible by Pi deficiency (Supplementary Fig. 1). Both are similar to the *E.coli* GlpT, a plasma membrane protein with G3P–Pi and Pi–Pi antiport activity[12]. Transiently expressing each of these putative GlpT proteins fused to green fluorescent protein (GFP) in rice protoplasts verified that they were located on the vacuolar membrane (Fig. 1a; Supplementary Fig. 3). Therefore, we name them *O. sativa* vacuolar phosphate efflux transporter 1 (OsVPE1; *Os04G46880*) and *O. sativa* vacuolar phosphate efflux transporter 2 (OsVPE2; *Os08G06010*) with reference to their proposed function.

Transmembrane and topology prediction indicated that there are 12 transmembrane domains in these OsVPE proteins with both amino and carboxyl terminals facing the cytosol (Fig. 1b). To verify the topology of the OsVPE proteins, we fused a pH-sensitive GFP to the different ends of each OsVPE protein. PEpHluorin is a fluorescent protein that loses fluorescence when the pH is lower than 6.2, while PRpHluorin remains fluorescent in the vacuole[16]. Chimeric proteins with the PEpHluorin tagged to the N terminus, C terminus and the central loop (loop 6) of OsVPE1 still displayed clear fluorescence signals at the vacuolar membrane in rice protoplasts, whereas PEpHluorin inserted in the first loop of OsVPE1 was not fluorescent (Fig. 1c). Furthermore, tagging the pH-insensitive PRpHluorin at the first loop of OsVPE1 still displayed fluorescence at the vacuolar membrane (Fig. 1c). These results indicate that the N terminus, C terminus and the central loop of each OsVPE protein faces the cytosol, and the first loop faces the vacuolar lumen, consistent with the topology prediction.

Quantitative real-time reverse transcription PCR analysis showed that the steady-state levels of *OsVPE1* and *OsVPE2* transcripts were 3–5 times higher in Pi starvation-stressed plants than in plants grown in replete Pi (Supplementary Fig. 4). Since rice PHOSPHATE STARVATION RESPONSE 1 (OsPHR1), OsPHR2 and OsPHR3 Myb transcription factors can bind to the PHR1-binding sequences (P1BS) to activate the transcription of Pi starvation-induced (PSI) genes[17], we further demonstrated that they were required for the low-Pi-induced expression of *OsVPE1* and *OsVPE2* (Supplementary Fig. 4). To determine where OsVPE1 and OsVPE2 accumulate in rice plants, we generated transgenic plants harbouring either the OsVPE1pro:gOsVPE1-GUS (β-glucuronidase) or the OsVPE2pro:gOsVPE2-GUS translational fusion proteins. Although both OsVPE1 and OsVPE2 reporters were active in the root and shoot tissues in plants grown under the Pi-replete (200 μM Pi) conditions, Pi deficiency (0 μM Pi) dramatically increased the levels of their expression (Fig. 1d,e). Under Pi-replete conditions, OsVPE1 was mainly expressed in the inner epidermis, the exodermis of the maturation zone of primary root and the vascular bundles in leaves (Fig. 1d). Under Pi-deficient conditions, high OsVPE1 protein levels were also observed in leaf mesophyll cells and epidermal, cortical cells and the stele of the maturation zone of primary root (Fig. 1d). Under Pi-replete conditions OsVPE2 was detected in the root cap, lateral root primordial and mesophyll cells in the leaf (Fig. 1e). But under Pi-deficient conditions, OsVPE2 protein levels were more highly expressed in leaf mesophyll cells and all root cells (Fig. 1e). Together, these data demonstrate that OsVPE1 and OsVPE2 are Pi starvation-induced vacuolar membrane proteins in rice.

**OsVPE1 and OsVPE2 mediate Pi membrane transport in yeast and *X. laevis* oocytes.** In *E.coli*, GlpT transports G3P into and Pi out of the cell and operates with a 1:1 stoichiometry[13]. To test whether OsVPE proteins can directly transport Pi across membranes, we expressed *OsVPE1* and *OsVPE2* driven by the ADH1 promoter in a yeast mutant strain (YP100) that is defective in Pi transport and does not grow unless supplemented with galactose[18]. While the YP100 mutant strains did not grow on YNB media (lacking galactose), transformation with the *ADH1:PHO84* (the high-affinity Pi transporter from yeast) transgene restores growth (Fig. 2a). Transformation of the YP100 strain with the yeast low-affinity transporter gene (*ADH1:PHO91*) also supported growth on media containing >10 mM Pi, while transformation with empty vector did not restore growth. Similarly, transformation of the YP100 strain with either *ADH1:OsVPE1* or *ADH1:OsVPE2* restored growth on media containing Pi concentrations above 10 mM, which indicated that net Pi uptake occurred in these strains. Together, these data imply that OsVPE1 and OsVPE2 can catalyse Pi transport across membranes.

To independently verify that VPE proteins transport Pi across membranes, we expressed the yellow fluorescen protein (YFP)–OsVPE2 fusion protein in *X. laevis* oocytes by microinjecting *YFP–OsVPE2* complementary RNA and measuring Pi transport. The YFP–OsVPE2 was targeted to the plasma membrane in oocytes (Fig. 2b). Oocytes expressing *YFP–OsVPE2* incubated with 5 mM Pi at pH 5.5 took up $^{33}$Pi at ~0.29 nmol h$^{-1}$ per oocyte compared with ~0.02 nmol h$^{-1}$ per oocyte in the water-injected control (Fig. 2c). Furthermore, increasing the pH of the bath solution to pH 7.5 reduced $^{33}$Pi uptake to ~0.13 nmol h$^{-1}$ per oocyte in the *YFP–OsVPE2*-expressing oocytes (Fig. 2c). This indicates that OsVPE2 is most active at acidic pH. Given that *E. coli* GlpT transports G3P into and Pi out of cells, we tested whether OsVPE2-mediated Pi uptake was coupled with the transport of G3P across membranes out of the cell (antiport). An analysis of sequence alignments showed that while the residues interacting with Pi were conserved in the *E. coli* GlpT and OsVPE proteins, those interacting with the glycerol moiety of G3P were not conserved[19] (Supplementary Fig. 5). This suggests that OsVPE proteins do not act as G3P–Pi antiporters. Consistent with this result, oocytes expressing *E. coli* GlpT displayed weak Pi uptake activity (Fig. 2d), and the injection of 5 mM G3P into these oocytes led to a Pi uptake comparable to that of OsVPE2. This demonstrates that the activity of the *E. coli* GlpT proteins is activated by G3P as expected for an antiporter protein. By contrast, addition of 5 mM G3P to oocytes expressing *YFP–OsVPE2* did not increase the Pi influx rate (Fig. 2d). These data are consistent with the structural data and demonstrate that OsVPE2 transports Pi across the vacuole membrane but is not a Pi–G3P antiporter. To estimate the permeability of OsVPE proteins to other anions, we measured the $^{33}$Pi uptake speed in the presence of other anions (malate, nitrate, sulfate or chloride) added to oocytes at a concentration 30 mM. The transport activity of OsVPE2 was not changed by the presence of other anions, while it was significantly inhibited by the presence of

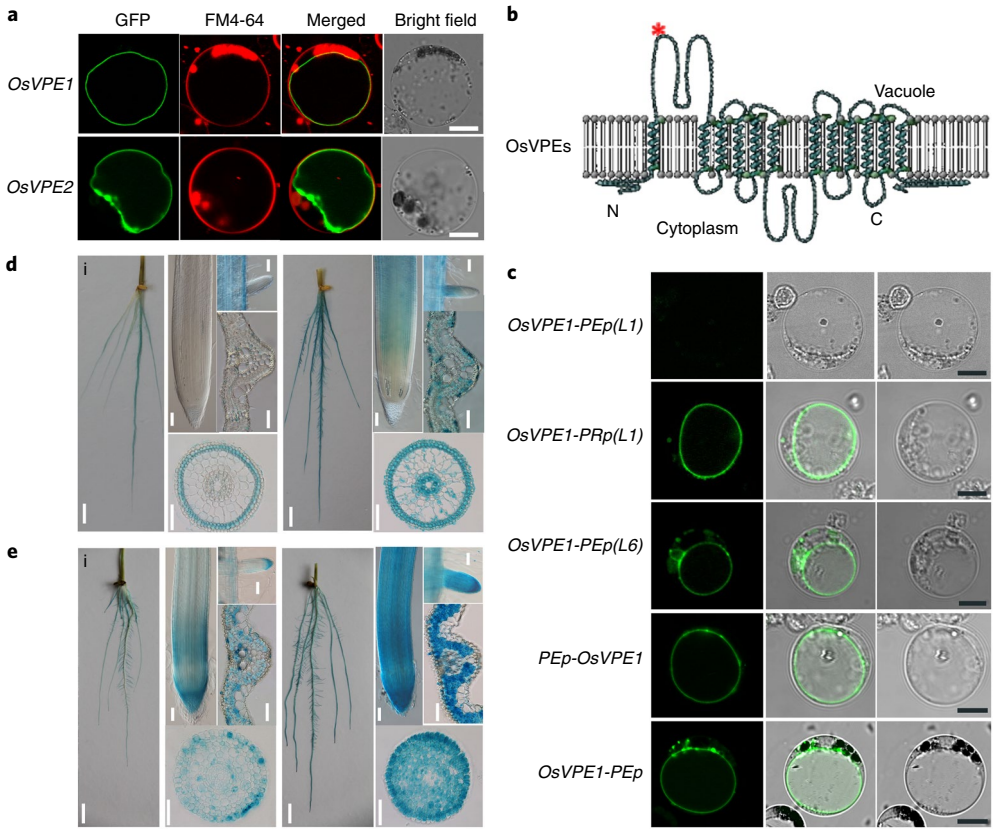


**Fig. 1 | A pair of Pi starvation-induced OsVPE proteins are located on the vacuolar membrane in rice. a**, Expression of *p35S:OsVPE1–GFP* and *p35S:OsVPE2–GFP* in rice protoplasts. The green signals indicate GFP, and the red signals indicate FM4-64 and autofluorescence of chlorophyll. Scale bar, 10 μm. **b**, Predicted topology profile of OsVPE proteins (made and displayed using the TMHMM and Topo2 software). The red asterisk indicates the position that the PEpHluorin and PRpHluorin fuse to the first loop of the OsVPE1 protein. **c**, Protoplasts of rice cells transiently expressing OsVPE1 fused with PEpHluorin or PRpHluorin as follows: *OsVPE1–PEP(L1)*, PEpHluorin was inserted into the first loop of OsVPE1; *OsVPE1–PRp(L1)*, PRpHluorin was inserted into the first loop of OsVPE1; *OsVPE1–PEp(L6)*, PEpHluorin was inserted into the sixth loop of OsVPE1; *PEp:OsVPE1*, PEpHluorin was fused to the N terminus (N) of OsVPE1; *OsVPE1–PEp*, PEpHluorin was fused to the C terminus (C) of OsVPE1. The green signals indicate GFP. Scale bar, 10 μm. **d**, GUS staining patterns of 8-day-old $P_{OsVPE1}$*:OsVPE1–GUS* transgenic plants grown under Pi-replete (200 μmol Pi) (left) and Pi-deficient conditions (0 μmol Pi) (right). Scale bars, 100 μm, 1 cm (i). **e**, GUS staining patterns of 8-day-old $P_{OsVPE2}$*:OsVPE2–GUS* transgenic plants grown under Pi-replete (200 μmol Pi) (left) and Pi-deficient conditions (0 μmol Pi) (right). Scale bars, 100 μm, 1 cm (i). For **a**, **c**–**e**, experiments were repeated three times and similar results were obtained.

30 mM cold Pi (Fig. 2e). A Michaelis–Menten analysis showed that the apparent mean $K_m$ value for Pi transport was 1.376 mM (Fig. 2f). These data demonstrate that OsVPE2 is a low-affinity Pi transporter and its transport activity is enhanced by the extracellular acidification in *X. laevis* oocytes.

Taken together, the restoration of Pi transport in yeast Pi transport mutants with rice VPE genes and the transport of Pi across plasma membranes in *X. laevis* oocytes that express *OsVPE2* suggest that OsVPE proteins are Pi transporters that facilitate Pi transport across the vacuolar membrane in rice.

**Overexpression of either *OsVPE1* or *OsVPE2* reduces Pi content in the vacuole.** To test whether OsVPE1 and OsVPE2 are vacuolar Pi transporters in rice, we generated transgenic rice plants overexpressing *OsVPE1* or *OsVPE2* under the transcriptional control of the 35S promoter and measured vacuolar Pi accumulation using NMR spectroscopy (Fig. 3a). Root vacuolar Pi content in lines overexpressing *OsVPE1* or *OsVPE2* were reduced to approximately ~20% of the level in the wild-type plants, whereas the cytoplasmic Pi content in these transgenic lines were similar to that in wild-type plants (Fig. 3b; Supplementary Fig. 6). Given that the vacuole is the major intracellular store for Pi, the reduction of vacuolar Pi also led to a reduced overall Pi content in the transgenic plants (Supplementary Fig. 6). We also generated transgenic rice plants overexpressing *GFP–OsVPE* fusions. The GFP–OsVPE proteins were localized on the vacuolar membrane in the transgenic plants, and the overall Pi content of the GFP fusion overexpressing lines were significantly lower than that in wild-type plants, which indicated that the GFP–OsVPE fusions are functional in planta (Supplementary Fig. 6). Furthermore, the growth of *OsVPE1*- or *OsVPE2*-overexpressing lines was less than the wild type under normal growth conditions. Because *OsVPE*-overexpressing lines accumulate lower levels of Pi in vacuoles than the wild type, the growth of the overexpressing lines was more severely reduced after transfer to a Pi-deficient condition compared with wild-type plants (Supplementary Fig. 6).

Together, these data are consistent with the hypothesis that OsVPE1 and OsVPE2 are vacuolar Pi transporters and facilitate Pi efflux from vacuoles.

**Disruption of OsVPE1 and OsVPE2 results in elevated vacuolar Pi content.** Given that OsVPE1 and OsVPE2 are transporters that actively efflux Pi from the vacuole, we predicted that the Pi content of vacuoles would be higher in mutant plants with disrupted OsVPE1 and OsVPE2 function. There was approximately 30–40%

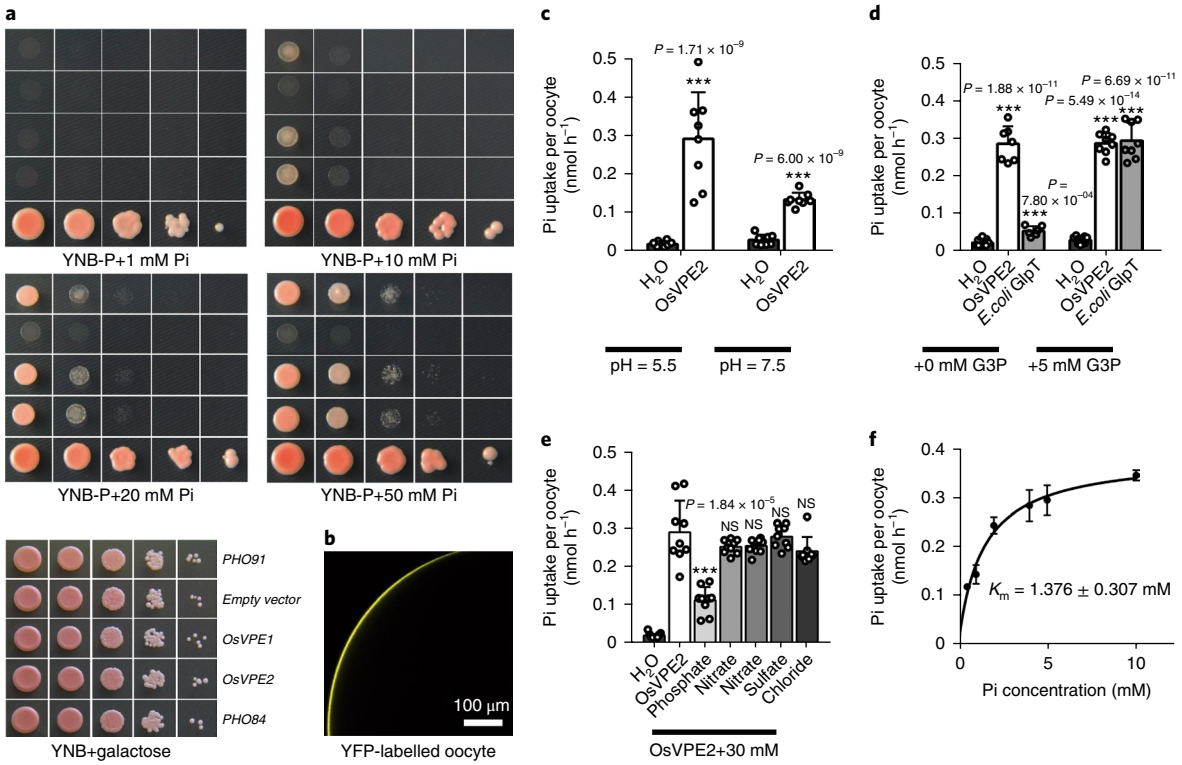


**Fig. 2 | OsVPE1 and OsVPE2 can confer Pi transport activity in yeast and *X. laevis* oocytes. a**, Complementation of the yeast mutant YP100 (Δ*pho84*Δ*pho87*Δ*pho89* Δ*pho90*Δ*pho91*Δ*git1*) expressing *OsVPE1* and *OsVPE2*. Equal volumes of tenfold serial dilutions were applied to YNB without phosphate (YNB-P; pH 5.5) medium with different Pi concentrations and incubated at 30 °C for 4 days. **b**, Subcellular localization of YFP–OsVPE2 in the oocyte membrane. **c**, OsVPE2-mediated Pi transport is dependent on $H^+$ in oocytes. *YFP–OsVPE2* cRNA or water-injected oocytes were incubated in Barth's solution without Pi for 2 days at 18 °C. Oocytes were transferred into Barth's solution containing 5 mM Pi with $^{33}P$ (1 mCi ml$^{-1}$ $H_3{}^{33}PO_4$), incubated in buffer at either pH 5.5 or 7.5 for 2 h. The asterisks indicate a significant difference between $H_2O$ and *OsVPE2* cRNA-injected oocytes. **d**, Transport activity of OsVPE2 is independent of G3P. *YFP–OsVPE2* cRNA, *E. coli GlpT* cRNA or water-injected oocytes were incubated in Barth's solution without Pi for 2 days at 18 °C. Oocytes were injected with 0 mM G3P or 5 mM G3P and transferred into Barth's solution (pH 5.5) containing 5 mM Pi with $^{33}P$ (1 mCi ml$^{-1}$ $H_3{}^{33}PO_4$) for 2 h. The asterisks indicate a significant difference between $H_2O$ and OsVPE2 or *E. coli GlpT* cRNA-injected oocytes. **e**, Anion selectivity of OsVPE2 in oocytes. Oocytes expressing *OsVPE2* or water-injected negative control were exposed to $^{33}P$ for 2 h at pH 5.5 in the external solution in the presence of 30 mM non-labelled Pi or 30 mM of other anions, including malate, nitrate, sulfate and chloride. The asterisks indicate a significant difference between *OsVPE2* cRNA-injected oocytes with and without 30 mM non-labelled Pi in external solution. **f**, $^{33}Pi$ uptake activity of oocytes injected with *OsVPE2* cRNA with different Pi concentrations in the external solution. For **c**–**f**, data are the means ± s.d. of $n = 8$ (**c**–**e**) or $n = 5$ (**f**); $^{***}P \leq 0.001$ by Student's *t*-test, two-tailed *t*-test; NS, not significant. All experiments were repeated three times, and similar results were obtained.

more Pi in the vacuoles of *Osvpe1-1* (a Tos-17 insertion mutant) and *Osvpe2-1* (a T-DNA insertion mutant) plants than in the wild-type plants (Supplementary Fig. 7). However, the cytoplasmic Pi content was similar in these loss-of-function mutants and in the wild type (Supplementary Fig. 7). The overall shoot and root Pi content were significantly higher in *Osvpe1-1* and *Osvpe2-1* mutants than in the wild-type plants because of the higher vacuolar Pi content in the mutants (Supplementary Fig. 7). The increased accumulation of Pi in these mutants was complemented by transformation with a genomic fragment containing *OsVPE1*, *OsVPE2* or *OsVPE2-GFP* in the *Osvpe1* or *Osvpe2* mutant, respectively (Supplementary Fig. 7). These data further support the hypothesis that OsVPE1 and OsVPE2 facilitate vacuolar Pi efflux and that the GFP–OsVPE fusions are functional. Furthermore, the growth of the *OsVPE1* or *OsVPE2* mutant was ~26% and ~28%, respectively, lower than the wild type (Supplementary Fig. 7). The decreased growth in these mutants demonstrated that vacuolar Pi efflux facilitated by OsVPE1 and OsVPE2 is required for growth.

To independently confirm the function of OsVPE1 and OsVPE2 in Pi efflux from the vacuoles, RNA interference (RNAi) and CRISPR–Cas9 (clustered regularly interspaced short palindromic repeats–CRISPR-associated protein 9) technologies[20] were used to generate *OsVPE1* and *OsVPE2* knockdown and knockout mutants. The root vacuolar Pi contents of *OsVPE1* and *OsVPE2* RNAi lines and a *Osvpe2-2* mutant (harbouring a 1-bp deletion at the target site that causes a frame shift) were higher than the wild type (Supplementary Figs. 7 and 8); this effect was also observed in the *Osvpe1-1* and *Osvpe2-1* mutants. Taken together, these data indicate that OsVPE1 and OsVPE2 are vacuolar Pi transporters and function in vacuolar Pi efflux and plant growth.

We also generated OsVPE1 and OsVPE2 double mutants to determine the role of these proteins in vacuolar Pi homeostasis. Under Pi-replete conditions, the root vacuolar Pi content and the overall shoot and root Pi content in the *Osvpe1-1 Osvpe2-2* double mutant were ~70% higher than those in the wild type, while the cytoplasmic Pi content of the double mutant was similar to the wild type (Fig. 3c,d; Supplementary Fig. 9). The vacuolar Pi content was higher in the double mutant than in either the *Osvpe1-1* or *Osvpe2-1* single mutants. Furthermore, the growth of the double mutant was much lower than in the single mutants (Fig. 4a,b). This suggests that OsVPE1 and OsVPE2 function additively in vacuolar Pi efflux and plant growth.

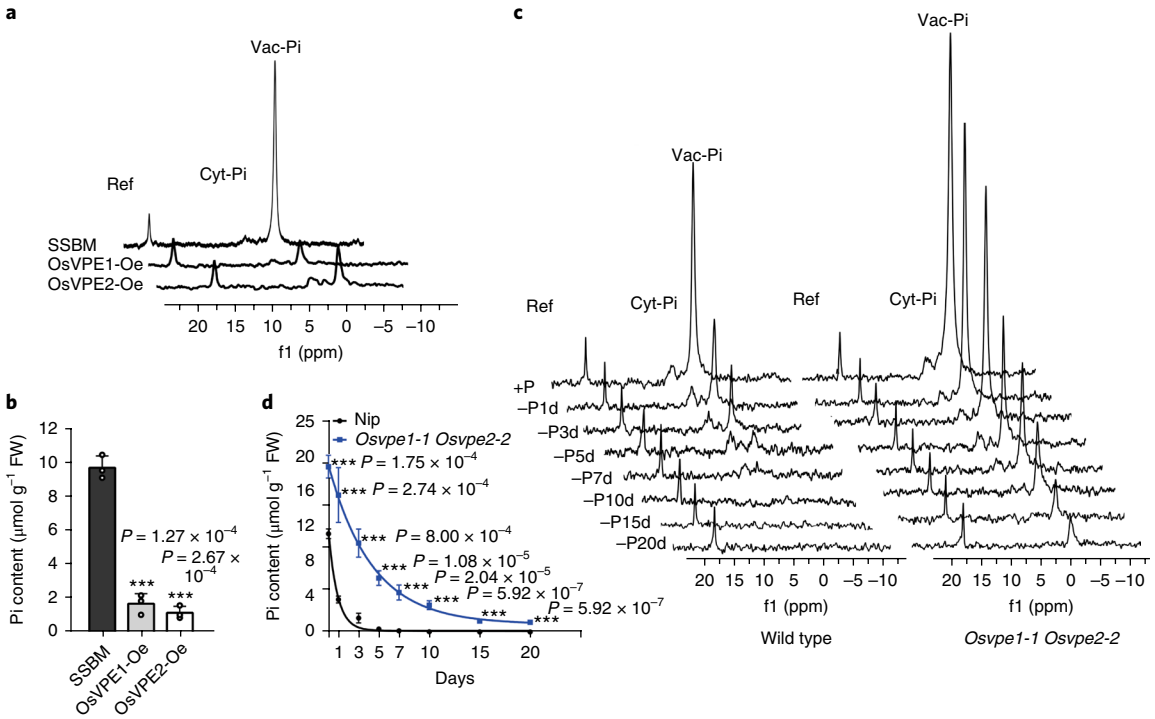


**Fig. 3 | Vacuolar Pi levels are significantly reduced in *OsVPE*-overexpressing plants and the efflux of vacuolar Pi in the *Osvpe1Osvpe2* double mutant is partially defective. a**, In vivo $^{31}$P-NMR spectra from roots of 14-day-old wild type (SSBM), and *OsVPE1* and *OsVPE2* overexpressing (Oe) lines grown under Pi-replete conditions (200 μmol Pi). Peaks from right to left are assigned to vacuolar Pi (Vac-Pi), cytoplasmic Pi (Cyt-Pi) and reference (Ref; methylenediphosphonate) used to measure chemical shifts and for quantification. **b**, The calculated Vac-Pi concentration of wild type, OsVPE1-Oe and OsVPE2-Oe plants. **c**, In vivo $^{31}$P-NMR spectra from roots of wild type (Nipponbare) and the double mutant (*Osvpe1-1 Osvpe2-2*) of 14-day-old seedlings grown under Pi-replete conditions (200 μmol Pi) were exposed to Pi starvation (0 μmol Pi) for different time periods. Peaks from right to left are assigned to Vac-Pi, Cyt-Pi and reference (methylenediphosphonate) used to measure chemical shifts and for quantifications. **d**, The calculated Vac-Pi concentration of wild type (Nip) and *Osvpe1-1Osvpe2-2* double mutant. The Vac-Pi of wild type could not be detected after 5 days of Pi starvation. For **b** and **d**, data are the means ± s.d. of $n = 3$ (**b**) or $n = 4$ (**d**); asterisks indicate a significant difference between wild type and overexpression lines (**b**) or *Osvpe1-1Osvpe2-2* (**d**); $^{***}P \leq 0.001$ by Student's *t*-test, two-tailed *t*-test. All expriments were repeated three times, and similar results were obtained. FW, fresh weight.

**Vacuolar Pi efflux in the OsVPE double mutant is lower than wild type.** Because OsVPE proteins catalyse Pi transport in yeast and *X. laevis* oocytes, and these proteins function in vacuolar Pi efflux, we further characterized the role of OsVPE proteins in vacuolar Pi efflux. Unfortunately, we did not detect distinct differences in current between the vacuoles of wild type, *Osvpe1-1 Osvpe2-2* double mutant and *OsVPE1*-overexpressing lines using patch-clamp experiments (Supplementary Fig. 10). Therefore, we used NMR spectrosopy to analyse and compare the root vacuolar Pi contents in the double mutant and the wild type plants over time after transfer to Pi-deficient conditions. The vacuolar Pi content of wild-type plants dropped quickly under Pi-starvation stress, with a ~67%, ~86% and ~97% reduction after 1, 3 and 5 days, respectively, of exposure to Pi starvation (from 11.73 ± 0.73 to 3.94 ± 0.38, 1.42 ± 0.32 and 0.27 ± 0.19 μmol Pi per g root, mean ± s.d., $n = 4$). After 7 days of starvation, vacuolar Pi was undetectable by NMR spectroscopy. By contrast, the root vacuolar Pi content of the *Osvpe1-1 Osvpe2-2* double mutant dropped more slowly than in the wild type. It decreased by ~17%, ~46% and ~67% after 1, 3 and 5 days, respectively of Pi starvation (from 19.0 ± 1.2 to 15.26 ± 2.86, 10.2 ± 1.46 and 6.5 ± 0.76 μmol Pi per g root, mean ± s.d., $n = 4$) (Fig. 3c,d). At the time point when the vacuolar Pi became undetectable by NMR spectroscopy in the wild type (7 days after Pi starvation), the vacuolar Pi content in the double mutant was 5.1 ± 0.8 μmol Pi per g root. This content is higher than in wild-type plants starved for a single day. Even after starvation for 15–20 days, the vacuolar Pi content was 1.16 ± 0.08 μmol Pi per g root, which was higher than the level of wild-type plants after 5 days of starvation. These data indicate that the release of stored Pi from vacuoles is slower in the *Osvpe1-1 Osvpe2-2* double mutant than in wild type. Together, these data indicate that OsVPE1 and OsVPE2 are vacuolar Pi efflux transporters.

**The OsVPE double mutant is hypersensitive to Pi starvation.** Because low-Pi stress-induced efflux of vacuolar Pi is delayed in the *Osvpe1-1 Osvpe2-2* double mutant, we predicted that compensation of cytoplasmic Pi levels by the vacuolar Pi store under starvation also might be slower in the double mutant than in the wild type. This would result in a defect in the growth response of the double mutant when grown in low phosphate conditions. To test this prediction, we transferred 2-week-old wild-type plants (Nipponbare) and *Osvpe1-1 Osvpe2-2* double mutant plants grown under Pi-replete conditions to Pi-starvation conditions for 2 weeks. Seedling growth of the double mutant was more severely inhibited compared with the wild-type plants (Fig. 4a,b). This demonstrates that the growth response of the double mutant under Pi starvation is defective.

If the low-Pi adaptive response was defective in the *Osvpe1-1 Osvpe2-2* double mutant, we would expect that the genes involved in Pi starvation signalling would be induced earlier in the double mutant than in the wild type. Steady-state transcript levels of the PSI genes *OsIPS1, OsPT6, OsSPX1* and *OsSQD2*[21–23] were measured in *Osvpe1-1 Osvpe2-2* and wild-type roots. The expression of *OsIPS1* and *OsSQD2* was slightly higher than in wild type, while the other PSI genes in *Osvpe1-1 Osvpe2-2* were expressed at similar levels to

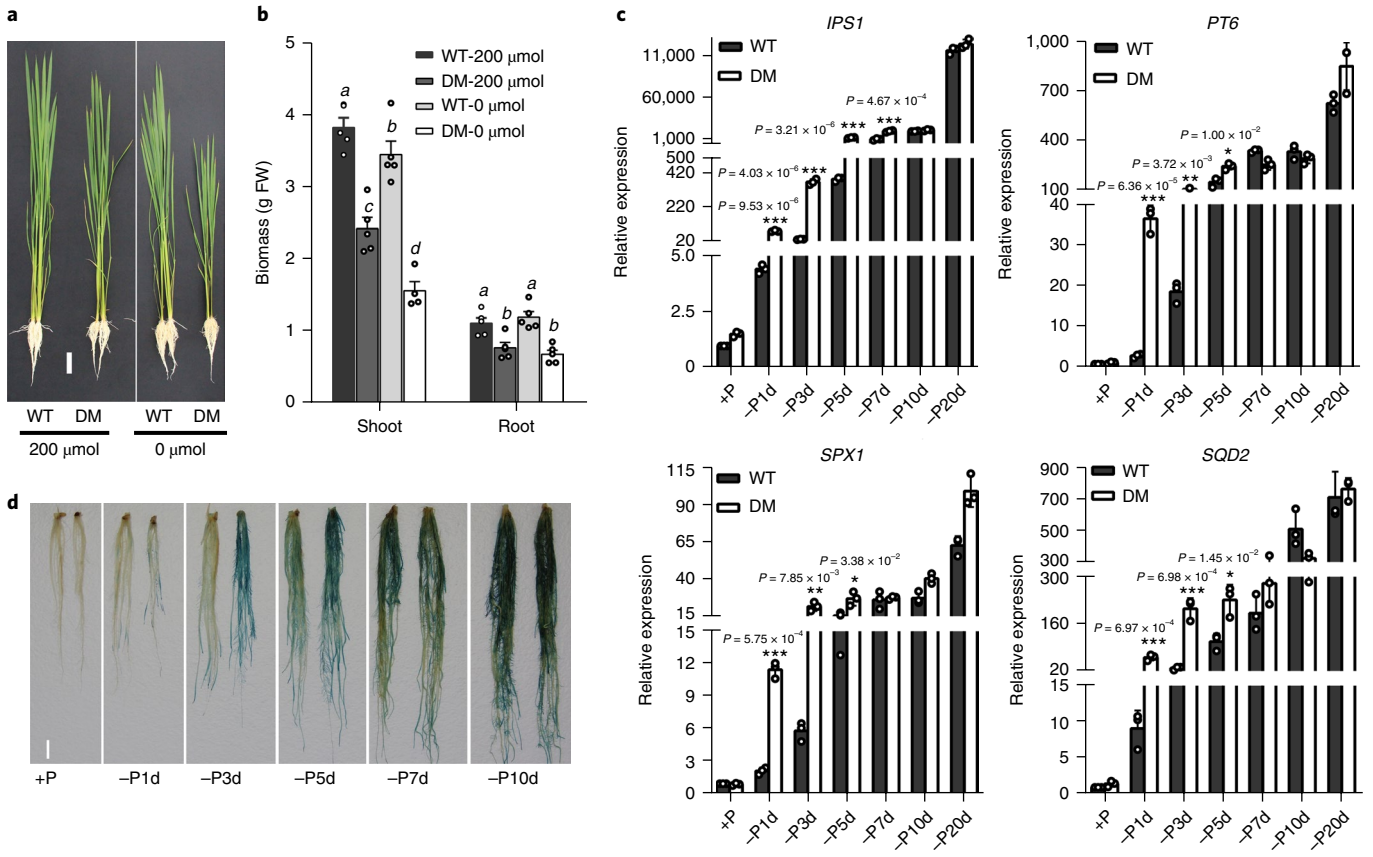


**Fig. 4 | The *Osvpe1Osvpe2* double mutant is stunted under Pi-replete conditions and more sensitive to Pi starvation. a**,**b**, Phenotype (**a**) and biomass (**b**) of 4-week-old wild-type (WT) and *Osvpe1Osvpe2* double mutant (DM) plants. The wild-type and double mutant plants were grown under Pi-replete conditions (200 μmol Pi) for 2 weeks and then transferred to Pi starvation conditions (0 μmol Pi) for another 2 weeks. Scale bar, 5 cm. Different letters in **b** indicate a significant difference between groups ($P < 0.05$ by Tukey's test). **c**, The induction of PSI genes is accelerated in the *Osvpe1-1Osvpe2-2* double mutant, as indicated by a comparison of the expression of PSR genes in roots between the wild-type and double mutant plants. Two-week-old wild-type plants and *Osvpe1-1Osvpe2-2* double mutant plants were grown under Pi-replete (+P) conditions (200 μmol Pi) and then exposed to Pi starvation (–P; 0 μmol Pi) for 1–20 days (1d–20d). The asterisks indicate a significant difference between wild-type and *Osvpe1-1Osvpe2-2* plants. *$0.01 < P \leq 0.05$, **$0.001 < P \leq 0.01$ and ***$P \leq 0.001$ by Student's *t*-test, two-tailed *t*-test. **d**, Histochemical analysis of GUS activity driven by 4xP1BS:GUS, a reporter gene containing a synthetic promoter harbouring four tandem copies of P1BS fused to the –46 minimal 35S promoter from cauliflower mosaic virus (4xP1BS). Scale bar, 1 cm. For each image, the wild type is on the left and the *Osvpe1-1Osvpe2-2* double mutant is on the right. For **b** and **c**, data are the means ± s.d., $n = 5$ (**c**) or $n = 3$ (**d**). All experiments used Nipponbare as the wild-type plants and were repeated three times, with similar results obtained.

the wild type under Pi-replete conditions (Fig. 4c). However, under Pi-deficient conditions, PSI gene transcripts increased more rapidly in the double mutant than in wild type. After 1 day and 5 days of Pi starvation, the expression levels of all PSI genes were significantly higher in *Osvpe1-1 Osvpe2-2* than in the wild type (Fig. 4c). However, after further starvation stress (from 10 to 20 days), the expression levels of all PSI genes were similar in the double mutant and in wild-type plants (Fig. 4c). This indicates that the onset of Pi stress is earlier in the *Osvpe1-1 Osvpe2-2* double mutant than the wild type. Consistent with this result, GUS activity of an artificial Pi-starvation reporter (4×P1BS:GUS)[24] was higher in the double mutant than in the wild type at the early stages (1–5 days) but was similar at later stages (7 days) during Pi starvation (Fig. 4d).

The increased growth inhibition and accelerated induction of PSI gene transcription by Pi starvation in the *Osvpe1-1 Osvpe2-2* double mutant compared with wild type suggests that OsVPE1 and OsVPE2 are vacuolar Pi efflux transporters and are required for Pi homeostasis and growth in rice experiencing low Pi stress.

**Angiosperm VPE and early diverging land plant GlpT proteins are located on the vacuolar membrane.** Given that the OsVPE proteins are vacuolar Pi efflux transporters in rice and similar to *E. coli* GlpT, and that the GlpT gene family is present in the genomes of both eukaryotes and prokaryotes[14], we examined the phylogenetic relationships between the vacuolar OsVPE proteins and the other GlpT proteins from plants. The rice genome contains four GlpT genes, *OsVPE1, OsVPE2*, *Os02g43620* and *Os06g08170*. We named the latter two as *OsGlpT1* (*Os02g43620*) and *OsGlpT2* (*Os06g08170*). We identified and retrieved GlpT sequences from 17 different land plant genomes and 2 chlorophyte genomes. Our analysis showed that there were early diverging land plant GlpT proteins and a single monophyletic group of spermatophyte (seed plant) GlpT proteins. A monophyletic angiosperm clade in turn comprised three monophyletic clades and each clade comprised proteins from most angiosperm taxa. This indicates that these three clades diverged from a common ancestor that existed sometime after the divergence of the lycophytes from the seed plant lineage. OsVPE1 and OsVPE2 together with GlpT proteins from 14 other angiosperm taxa form a monophyletic clade (VPE clade) that also includes three *Arabidopsis thaliana* proteins (At3g47420 (*AtVPE1/AtG3Pp1*), AT4G25220 (*AtVPE2/AtG3Pp2*) and At1G30560 (*AtVPE3/AtG3Pp3*)[14]) and no other rice members (Fig. 5a). There

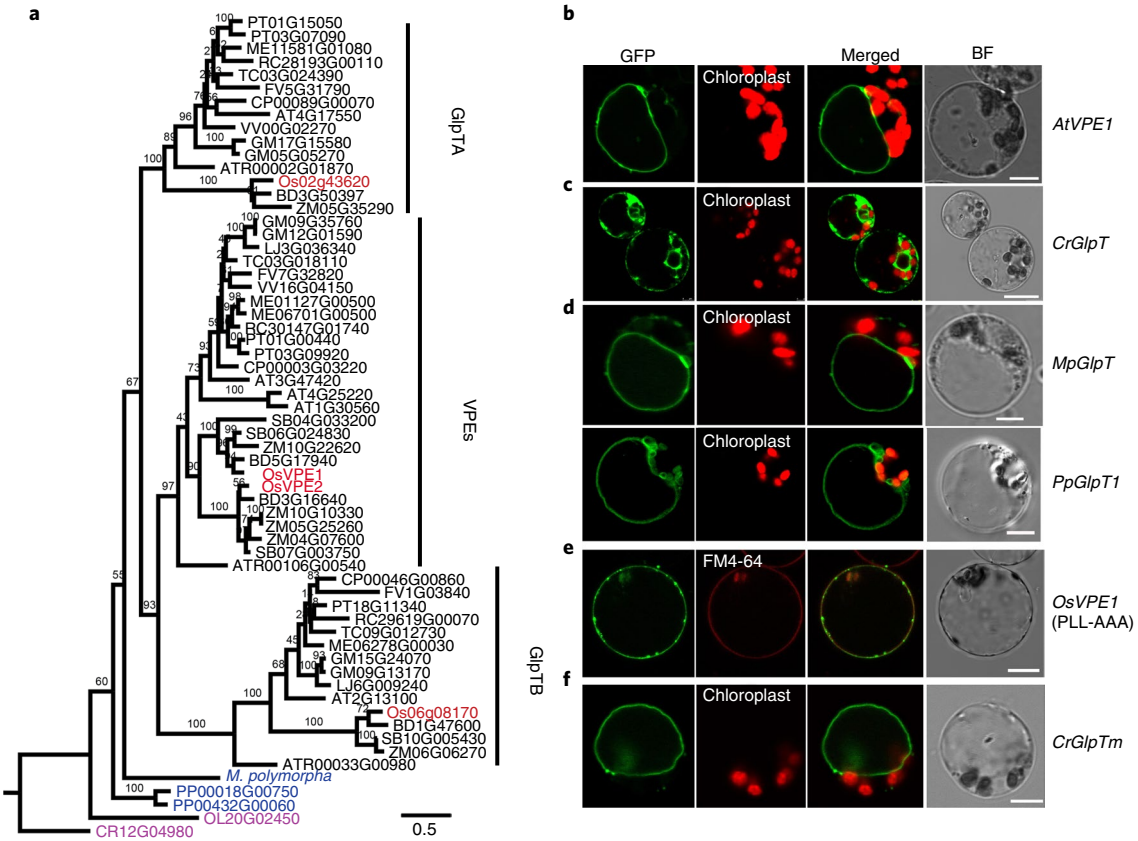


**Fig. 5 | OsVPE1 and OsVPE2 together with the relative GlpT form a separate VPE clade and reside on the vacuolar membrane in rice. a**, Maximum-likelihood phylogenetic analysis using GlpT sequences from 19 different plant species. The different colours indicate different species: purple, chlorophyte; blue, early land plants; black, angiosperm; and red, *O. sativa*. The scale bar represents branch length. Letters in the codes represent species names as follows: AT, *A. thaliana*; ATR, *Amborella trichopoda*; BD, *Brachypodium distachyon*; CP, *Carica papaya*; CR, *C. reinhardtii*; FV, *Fragaria vesca*; GM, *Glycine max*; LJ, *Lotus japonicus*; ME, *Manihot esculenta*; OL, *O. lucimarinus*; Os,*O. sativa*; PP, *P. patens*, PT, *Populus trichocarpa*; RC, *Ricinus communis*; SB, *Sorghum bicolor*; TC: *Theobroma cacao*; VV, *Vitis vinifera*, ZM, *Zea mays*. **b**, Expression of *p35S:AtVPE1–GFP* in *Arabidopsis* protoplasts. **c**, Expression of *p35S:CrGlpT–GFP* in rice protoplasts. **d**, Expression of *p35S:MpGlpT–GFP* (*M. polymorpha*) and *p35S:PpGlpT1–GFP* (*PP00018G00750*) in rice protoplasts. **e**, Replacing the dileucine motif with three alanine residues (PLL-AAA) resulted in the modified protein being guided to the plasma membrane. **f**, Replacing the central loop of CrGlpT with that from OsVPE1 mistargeted it to the vacuolar membrane. *CrGlpTm* indicates that the sixth loop of the CrGlpT protein was replaced by the sixth loop of OsVPE1. For **b**–**f**, the green signals indicate GFP and the red signals indicate autofluorescence of chlorophyll (**b**, **d**, **f**) or FM4-64 (**e**). Scale bar, 10 μm (**b**–**f**). All experiments were repeated three times, and similar results were obtained.

is a conserved dileucine signature for vacuolar membrane localization[25] in the predicted loop between the transmembrane domains 6 and 7 in almost all VPE members (Supplementary Fig. 11). Removal of the dileucine signature in OsVPE1 leads to mistargeting of the OsVPE1mut–GFP fusion to the plasma membrane (Fig. 5e). This suggests that the VPE proteins (including OsVPE1 and OsVPE2) are probably vacuolar membrane proteins. Consistent with this conclusion, transient expression of the putative vacuolar *Arabidopsis* VPE–GFP fusion proteins indicated that all three are located on the vacuolar membrane (Fig. 5b; Supplementary Fig. 12). The vacuolar Pi content of *Atvpe2-1* was 1.2-fold higher than that of the wild type (Supplementary Fig. 13). Together, our data indicate that the vacuolar GlpT proteins form a monophyletic clade among angiosperm GlpT proteins and may facilitate vacuolar Pi efflux.

The other angiosperm GlpT proteins form two distinct monophyletic clades, the GlpTA and GlpTB clades. There is no conserved signature for vacuolar membrane localization in the predicted loop between transmembrane domains 6 and 7 in proteins of either of these clades. This suggests that GlpTA and GlpTB proteins are not located on the vacuolar membrane. Consistent with this result, we found that GFP fusion proteins of OsGlpT1 (a GlpTA member) and OsGlpT2 (a GlpTB member) were predominantly localized at the endoplasmic reticulum and the plasma membrane, respectively (Supplementary Fig. 12). Given that the prokaryotic GlpT proteins are plasma membrane proteins, the subcellular localization of proteins in the three different clades suggests that subcellular relocalization to the vacuolar membrane of members of the VPE clade proteins may have occurred during the course of plant evolution.

Similar to the VPE proteins in angiosperms, a dileucine-based motif for vacuolar membrane localization was also present in the predicted loop between transmembrane domains 6 and 7 of the early diverging land plant GlpT proteins (Supplementary Fig. 11), and GlpT–GFP fusion proteins of *Marchantia polymorpha* and *Physcomitrella patens* were clearly located on the vacuolar membrane (Fig. 5d). This suggests that the GlpT proteins of the common ancestor of land plants were located on the vacuolar membrane.

However, no dileucine vacuolar membrane localization signature was identified in the predicted loop between transmembrane domains 6 and 7 of chlorophyte (*Chlamydomonas reinhardti* and *Ostreococcus lucimarinus*) GlpT proteins (Supplementary Fig. 11). Transient expression of the *C. reinhardtii* GlpT–GFP fusion in protoplasts resulted in a fluorescent signal at the endoplasmic reticulum

(Fig. 5c; Supplementary Fig. 12). Furthermore, replacing the central loop of CrGlpT by that of OsVPE1 targeted the chimeric protein to the vacuolar membrane (Fig. 5f). These data suggest that vacuolar targeting of the GlpT proteins occurred through the acquisition of the dileucine vacuolar-targeting signature in a common ancestor of land plants after the divergence of land plants and chlorophytes.

Together, these data indicate that vacuolar membrane localization is ancient in land plant GlpT proteins, which probably evolved from endoplasmic reticulum- or plasma membrane-localized GlpT proteins among ancestors of land plants. These vacuolar GlpT proteins are essential for vacuolar Pi efflux in land plants, a key adaptation to life in the patchy terrestrial environment.

## Discussion

Pi is an essential nutrient for plant growth and plants have evolved a complex battery of transporters to regulate Pi uptake and homeostasis. After acquisition by the root, excess Pi is stored in vacuoles from which it can be remobilized into the cytosol on demand. Although vacuolar transporters must facilitate vacuolar Pi efflux under Pi starvation[26], the molecular nature of Pi transporters that release vacuolar Pi into the cytoplasm remained unclear. Here, we showed that a pair of vacuolar membrane proteins, OsVPE1 and OsVPE2, are functional Pi membrane transporters required for Pi efflux from the vacuole into the cytoplasm in rice. Vacuolar Pi content is higher in rice mutants that lack OsVPE1 and OsVPE2 function than in wild type. Furthermore, depletion of vacuolar Pi stores in mutants under Pi starvation is slower than in Pi-starved wild type plants. This delayed supply of Pi to the cytoplasm in Pi-stressed mutants causes early onset of PSI gene expression. Our data support the conclusion that the OsVPE proteins are essential transporters for vacuolar Pi efflux and play crucial roles in the release of vacuolar Pi into the cytoplasm to satisfy the cellular Pi requirements and growth under Pi-starvation stress.

The OsVPE proteins belong to the GlpT family that transports G3P into and Pi out of the *E. coli* cell and operates with a 1:1 stoichiometry[13]. However, our data suggest that the OsVPE proteins function as Pi transporter on the vacuolar membrane in plants and do not function as G3P–Pi antiporters. There are two pieces of evidence that support this view. First, expressing *OsVPE2* in oocytes induces Pi influx, but this transport is not affected by the presence of G3P in the cell (Fig. 2d). Second, the G3P concentration in plant protoplasts is relatively low and little accumulates in vacuoles[27]. If VPE transports G3P into vacuoles and Pi to the cytoplasm, an increase in the amount of G3P or its metabolites would be observed in Pi-starved plants. Such increases have not been observed[28]. The mechanism of Pi transport without movement of G3P by OsVPE proteins can be explained by a recent study of the atomic-level characterization of transport cycle thermodynamics for the *E.coli* GlpT. It showed that the free energy of the outward-facing state of *E.coli* GlpT is higher than that of the inward-facing state in the absence of G3P[29]. Therefore, in the absence of G3P, cytosol-facing VPE on the vacuolar membrane may release the bound Pi without accepting a counter ion such as G3P and switch back into the vacuolar lumen-facing state to further bind Pi in the vacuole given additional energy (for example, high Pi and proton gradients across the vacuolar membrane) to overcome the transition barrier. In this way, the Pi starvation-induced expression of OsVPE proteins could favour the efflux of high concentration Pi from the vacuole to buffer cytoplasmic Pi concentrations.

Our data indicate that OsVPE proteins may function as low-affinity Pi transporters in planta. Low-affinity Pi transporters are needed to facilitate vacuolar Pi efflux when the plants were subjected to Pi-starvation stress because the vacuolar Pi content in wild-type plants grown in sufficient Pi was approximately 10–20 μmol Pi per g root (~10–20 mM Pi). Our results showed that OsVPE proteins are crucial for this process, because overexpression of OsVPE proteins in plants grown under Pi-sufficient conditions exhibited a reduced root vacuolar Pi concentration to 1.5–2 mM. Furthermore, vacuolar Pi efflux in the *Osvpe1-1 Osvpe2-2* double mutant was delayed when the plants were transferred from Pi-sufficient conditions to Pi starvation (Fig. 3c,d). These data are consistent with the evidence that OsVPE proteins operate in the low-affinity range in oocytes (Fig. 2f). However, under long-term Pi starvation stress, the vacuolar Pi store was depleted. This indicates that high-affinity Pi transporters are also required for the efflux of Pi from vacuoles when the Pi concentration drops below the millimolar range. The stabilization of the vacuolar Pi concentration to ~1.1 mM Pi in *Osvpe1-1 Osvpe2-2* double mutant roots under long-term Pi starvation stress indicates that OsVPE proteins are also required either for high-affinity efflux directly or for the activation of other unidentified high-affinity vacuolar Pi efflux transporters under starvation.

Several recent studies have identified a class of SPX-MFS proteins as vacuolar Pi transporters. These proteins, referred to as VPT or PHT5 in *Arabidopsis*, are vacuolar Pi influx transporters. Vacuolar Pi contents are higher in lines overexpressing the *VPT1*/*PHT5;1* gene, while vacuolar Pi contents are lower in *vpt1*/*pht5;1* loss-of-function mutants than in wild-type plants[9,10]. In the *Arabidopsis vpt1* mutant, the vacuolar Pi influx activity is significantly reduced, supporting the notion that VPT1 is an influx transporter[9]. Furthermore, OsSPX-MFS1, a homologue of VPT1/PHT5 from rice, can complement the *pht5* mutant in *Arabidopsis*, suggesting that the OsSPX-MFS family of proteins may also function as vacuolar Pi influx transporters[10]. However, another study[11] suggested that OsSPX-MFS3 may function as a vacuolar Pi efflux transporter because overexpression of *OsSPX-MFS3* leads to a lower vacuolar Pi content in rice. By contrast, we showed that overexpression of *GFP–OsSPX-MFS3* leads to a greater than twofold increase of vacuolar Pi content. Furthermore, the vacuolar Pi content is significantly lower in the *OsSPX-MFS3* loss-of-function mutants than in wild type (Supplementary Fig. 2). Therefore, both our gain-of-function and loss-of-function data indicate that OsSPX-MFS3 is a vacuolar Pi influx transporter. Consistent with the proposed function of OsSPX-MFS3 as a vacuolar Pi influx transporter is the observation that both steady-state *OsSPX-MFS3* transcript levels and OsSPX-MFS3 protein levels are repressed by Pi-starvation stress in rice[30] (Supplementary Fig. 1), while the proteins are required for Pi sequestration in the vacuole under Pi-sufficient conditions. If OsSPX-MFS3 is a vacuolar Pi influx transporter, our results indicate that the VPE proteins we identified here are vacuolar Pi efflux transporters in plants. Not only do VPE proteins function as vacuolar Pi efflux transporters in rice but the *Arabidopsis* VPE proteins also function in vacuolar Pi efflux. This is because the vacuolar Pi content is higher in the Arabidopsis *Atvpe2* mutant than in wild type. Future analyses of the coordination of the activity of SPX-MFS proteins and VPE proteins are required to understand vacuolar Pi homeostasis in plants.

Our findings suggest that the VPE proteins and the GlpT proteins from early diverging land plants were selected as transporters to remobilize Pi from the vacuolar Pi store in the cytoplasm at or before the evolution of land plants. The vacuole is a major compartment for phosphorus storage and remobilization. In fungi and chlorophytes, phosphorus is stored in vacuoles in the form of inorganic polyphosphate. However, Pi is the major storage form of phosphorus in vacuoles of higher plants. The difference in storage forms of phosphorus in vacuoles indicates that divergent strategies are required for vacuolar phosphorus homeostasis in fungi, algae and plants. Likewise, the VPE proteins and the GlpT proteins from early diverging land plants were recruited to the vacuolar membrane for vacuolar Pi efflux in a common ancestor of the land plants. Furthermore, the amino acid residues required for Pi selectivity in *E. coli* GlpT were conserved in the VPE and the GlpT proteins from early diverging land plants. Amino acid motifs that recognize and

bind the glycerol moiety of G3P are not present in the VPE and the GlpT proteins from early diverging land plants (Supplementary Fig. 5). Therefore, these proteins may have been recruited to the vacuolar membrane as a Pi transporter in streptophyte algae before the evolution of land plants. Since GlpT proteins are not located on the vacuolar membrane in chlorophytes, it is likely that unrelated proteins are required for the release of phosphorus from vacuoles in chlorophyte algae. Identification of all the vacuolar Pi transporters in chlorophytes and streptophytes may shed light on the evolution of phosphorus storage and remobilization in Viridiplantae.

Together, our evidence demonstrates that the recruitment of an ancient plasma membrane GlpT to the vacuolar membrane enabled the evolution of a vacuolar Pi efflux process that is central to land plant Pi homeostasis. This mechanism allowed plants to achieve high growth rates in the terrestrial environment, where phosphorus availability is patchy and limiting to growth. The presence of the VPE family in extant, early diverging land plants indicates that this physiological adaptation would have evolved among the common ancestors of land plants before or soon after colonization during the Ordovician period.

## Methods

**Genotyping and growth conditions.** The homozygous lines of the T-DNA (PFG_3A-60568.L) and To17 (T41731T) insertion were screened by PCR using the primers listed in Supplementary Table 1. Hydroponic experiments were conducted as described previously[31]. All the plants were grown in a greenhouse with a 12-h day (30 °C)/12-h night (22 °C) photoperiod, approximately 200 μmol $m^{-2}$ $s^{-1}$ photon density, and approximately 60% humidity.

*A. thaliana* wild type (Columbia-0) and the T-DNA insertion mutant line (*Atvpe2-1*, GABI_179F04, At4G25220) were obtained from the Arabidopsis Stock Center. Homozygous individuals were screened by PCR using the primers listed in Supplementary Table 1. Seeds were surface sterilized and germinated on 0.5 Murashige and Skoog medium, supplemented with 1.5% (w/v) sucrose and 1.2% (w/v) agar.

**Vacuolar membrane proteomic analysis.** The roots of 8-day-old rice seedlings grown on culture medium supplemented with 200 μM Pi or 0 μM Pi were sampled. Rice vacuolar membranes were isolated following previously published methods[32].

For digestion, the protein solution was reduced with 10 mM dithiothreitol for 1 h at 37 °C and alkylated with 20 mM iodoacetamide for 45 min at room temperature in darkness. For trypsin digestion, the protein sample was diluted by adding 100 mM triethylammonium bicarbonate (TEAB) to urea to a concentration less than 2 M. Finally, trypsin was added at 1:50 trypsin-to-protein mass ratio for the first digestion overnight and 1:100 trypsin-to-protein mass ratio for a second 4-h digestion. Approximately 100 μg protein for each sample was digested with trypsin for subsequent experiments.

After trypsin digestion, peptide samples were desalted using a Strata X C18 SPE column (Phenomenex) and vacuum-dried. Peptide samples were reconstituted in 0.5 M TEAB and processed according to the manufacturer's protocol for 8-plex iTRAQ Reagent. $iTRAQ_{113}$ and $iTRAQ_{114}$ were used to label the peptides from Pi-replete and Pi-deficienct conditions. Briefly, one unit of iTRAQ reagent (defined as the amount of reagent required to label 100 μg of protein) was thawed and reconstituted in 24 μl acetonitrile. The peptide mixtures were then incubated for 2 h at room temperature and pooled, desalted and dried by vacuum centrifugation.

The sample was then fractionated via high pH reverse-phase high-performance liquid chromatography using an Agilent 300Extend C18 column (5-μm particles, 4.6-mm ID, 250-mm long). Briefly, peptides were first separated with a gradient of 2% to 60% acetonitrile in 10 mM ammonium bicarbonate pH 8 over 80 min into 80 fractions, Then, the peptides were combined into 18 fractions and dried by vacuum centrifuging.

Peptides were dissolved in 0.1% formic acid, directly loaded onto a reversed-phase pre-column (Acclaim PepMap 100, Thermo Scientific). Peptide separation was performed using a reversed-phase analytical column (Acclaim PepMap RSLC, Thermo Scientific). The gradient comprised an increase from 6% to 22% solvent B (0.1% formic acid in 98% acetonitrile) over 24 min, 22% to 36% in 8 min and climbing to 80% in 4 min then holding at 80% for the last 4 min, all at a constant flow rate of 280 nl $min^{-1}$ on an EASY-nLC 1000 UPLC system, the resulting peptides were analysed using a Q Exactive Plus hybrid quadrupole-Orbitrap mass spectrometer (ThermoFisher Scientific). The peptides were subjected to a nanospray ionization source followed by tandem mass spectrometry (MS/MS) in Q Exactive Plus (Thermo) coupled online to the ultra-performance liquid chromatography system. Intact peptides were detected in the Orbitrap at a resolution of 70,000. Peptides were selected for MS/MS using a normalization collision energy (NCE) setting of 30; ion fragments were detected in the Orbitrap at a resolution of 17,500. A data-dependent procedure that alternated between one MS scan followed by 20 MS/MS scans was applied for the top 20 precursor ions above a threshold ion count of 2E4 in the MS survey scan with 30.0 s dynamic exclusion. The electrospray voltage applied was 2.0 kV. Automatic gain control (AGC) was used to prevent overfilling of the ion trap; 5E4 ions were accumulated for the generation of MS/MS spectra. For MS scans, the $m/z$ scan range was 350 to 1,800. The fixed first mass was set as 100 $m/z$. The resulting MS/MS data were processed using Mascot search engine (v.2.3.0).

**Plasmid construction and plant transformation.** To generate transgenic lines overexpressing various OsVPE proteins, the open reading frames of genes encoding the OsVPE proteins were introduced into the binary vector pCAMBIA 1300 following the cauliflower mosaic virus 35S promoter using the restriction enzyme sites BamHI and SalI. For the RNAi vector construction, a 217-bp and 201-bp fragment of *OsVPE1* and *OsVPE2* were amplified, respectively, and cloned into pENTRTM/D-TOPO vectors (Life Technologies) and subsequently recombined into the destination vector pH7GWIWIG2 according to the manufacturer's instructions. Primer sequences are listed in Supplementary Table 1.

To generate GUS reporter lines, the genome fragments of *OsVPE1* and *OsVPE2* were amplified and introduced into the pCAMBIA 1300-GUS plasmid between BamHI and SalI sites. Primer sequences are listed in Supplementary Table 1.

To generate complementation lines for the *Osvpe1-1* and *Osvpe2-1* mutants, the genomic fragments (containing the 3,000-bp promoter) of *OsVPE1* and *OsVPE2* were amplified and inserted into the modified binary vector pCAMBIA 2300. The fragment of *OsVPE1* was introduced into the KpnI and SalI sites, and fragment *OsVPE2* was introduced into the SacI and BamHI sites. Primer sequences are listed in Supplementary Table 1.

The *Osvpe2-2* and *Osspx-mfs3* CRISPR vectors were constructed following previously published protocols[20] using the primers listed in Supplementary Table 1.

For subcellular localization analysis, the open reading frames of *OsVPE1*, *OsVPE2*, *OsGlpT1*, *OsGlpT2*, *CrGlpT*, *AtVPE1, AtVPE2*, *AtVPE3*, *PpGlpT1* and *MpGlpT* were introduced into the pCAMBIA 1300 vector containing the 35S promoter and the GFP fragment. The open reading frames of *OsVPE1*, *OsVPE2*, *OsGlpT1* and *OsGlpT2* were amplified and introduced into the SacI and SalI sites. The open reading frames of *CrGlpT*, *AtVPE1*, *AtVPE3* and *PpGlpT1* were introduced into the KpnI and SalI sites. The open reading frame of *AtVPE2* was introduced into the KpnI and SmaI sites. The open reading frame of *MpGlpT* was introduced into the BamHI and SalI sites. GFP was fused to the C terminus of these genes. Primer sequences are listed in Supplementary Table 1.

To generate transgenic lines overexpressing *OsSPX-MFS3*, the open reading frame of *OsSPX-MFS3* was introduced into the binary vector pCAMBIA 1300 following the cauliflower mosaic virus 35S promoter and the GFP fragment using the restriction enzyme sites KpnI and SalI. GFP was fused to the N terminus of *OsSPX-MFS3*. Primer sequences are listed in Supplementary Table 1.

Plant transformation was conducted through *Agrobacterium tumefaciens* (strain EHA105)-mediated transformation as previously described[31].

**Quantitative real-time PCR analysis.** Total RNA was extracted from plant samples using RNeasy Mini kits (Qiagen) and reverse transcribed to complementary DNA after DNase I treatment using a SuperScript II kit (Invitrogen) following the manufacturer's instructions. Quantitative real-time PCR was performed using a SYBR Premix kit (Roche) on a QuantStudio 6 Flex machine (Life Technologies). The rice *OsActin* gene was used as an internal control. Primer sequences are listed in Supplementary Table 1.

**Histochemical localization of GUS expression.** For GUS staining, the tissues were incubated in a solution containing 50 mM sodium phosphate buffer (pH 7.0), 5 mM $K_3Fe(CN)_6$, 5 mM $K_4Fe(CN)_6$, 0.1% Triton X-100 and 1 mM X-Gluc at 37 °C. Sections (35 μM) of various plant tissues were produced using a vibratome (Leica VT 1000S). Images were taken using a camera (Nikon) or microscope (Nikon ECLIPSE Ni).

**Subcellular analysis of VPE–GFP fusions.** The GFP fusion plasmids were transformed into protoplasts by polyethylene glycol-mediated transformation. Protoplast preparation and transfection followed previously described procedures[33,34]. An endoplasmic reticulum localized marker was used for colocalization analyses[35]. FM4-64 (5 μM, staining for 5–10 min) was used as the indicator of plasma membranes. Confocal microscopy images were taken using a laser scanning confocal microscope (Leica TCS SP5). Excitation and emission wavelengths Ex488/Em500-550, Ex516/Em630-700 and Ex516/Em600-650 were used for GFP, autofluorescence of chlorophyll and FM4-64, respectively.

**Measurements of Pi content and $^{31}$P-NMR analysis of vacuolar and cytoplasmic Pi.** For Pi measurements, shoots and roots were collected separately and then ground into powder in liquid nitrogen. $H_2S0_4$ (500 μl, 5 mol per litre) was added to a 1.5-ml Eppendorf tube with ~0.05 g powder. The Pi content was measured following a previously described procedure[31].

Approximately 0.07 g rice roots were used for NMR analysis. The roots were packed into a 5-mm-diameter NMR tube equipped with a perfusion system (5 mM glucose, 10 mM $KNO_3$, 0.5 mM $Ca(NO_3)_2$, 1 mM KCl, 0.5 mM $MgSO_4$, 200 or 0 μM

$KH_2PO_4$, 2 mM MES, pH 5.5) connected to a peristaltic pump. $^{31}$P-NMR spectra were recorded on a standard broadband 5-mm probe on a Bruker Ascend 600 spectrometer with TopSpin software v.3.0. The $^{31}$P-NMR spectra were recorded at 242.9 MHz lock with deuteroxide in two 0.5-mm glass capillaries. The $^{31}$P-NMR acquisition conditions were as follows: 30° radiofrequency pulses (70 µs) at 2 s relaxation delay; 24 KHz spectral width; Waltz-based broadband proton decoupling (44 W during acquisition time, 0.6 W during delay) with a probe temperature of 25 °C. Free induction decays (FIDs) were collected as 16 K data points, zero-filled to 32 K, and processed with a 30-Hz exponential line broadening. Each spectrum was acquired over 0.34 s and was the sum of 4,500 scans. The resonance assignments are as follows: reference, a 0.3-mm glass capillary containing 10 mM methylene diphosphonate, which was at 18.85 ppm relative to the signal from 85% $H_3PO_4$; the reference was then used to measure chemical shifts and for quantifications. To quantify the vacuolar and cytoplasmic Pi, a calibration curve was obtained by using Pi solutions of various concentrations.

**Transport activity assay in yeast.** To generate vectors for yeast complementation, the coding region of *PHO84*, *OsVPE1*, *OsVPE2* and *PHO91* were introduced into the BamHI and NotI sites on the PRS426–ADH1 vector. Primers for vector constructs are listed in Supplementary Table 1. These constructs and empty vector were transformed into the strain YP100. Transformants were selected on uracil-deficient medium and grown in synthetic complete (SC-uracil) yeast medium containing 2% galactose, 0.67% yeast nitrogen base without amino acids, 0.2% appropriate amino acids and 2% agar at pH 5.5 and incubated at 30 °C for 3–4 days. One colony was selected from each transformation strain and grown in the liquid SC-uracil medium. The mid-exponential phase cells were collected and washed three times with water, and resuspended to $OD_{600} = 1$. Equal volumes of tenfold serial dilutions were spotted to YNB medium (without phosphate) with 2% glucose, 2% agar, appropriate amino acids and different Pi concentrations. Plates were incubated at 30 °C for 4 days.

**Transport activity assay in *X. laevis* oocytes.** *OsVPE2* cDNA that was already optimized according to *X. laevis* codon preferences was cloned into the nYFP-pNB1 vector for expression in oocytes using the USER method[36]. cRNA synthesis was performed from ~1 µg of linearized plasmid DNA template using a mMessage mMachine T7 kit (Ambion). Synthesis lasted for 2 h at 37 °C and cRNA was purified using a MEGA clear Transcription Clean-Up kit (Invitrogen). Healthy oocytes at stage IV and V were selected for injection with 25 ng cRNA or the same amount of water. Injected oocytes were incubated in Barth's solution at 18 °C for 2 days. The incubation solution was refreshed daily. The Barth's solution contained 96 mM NaCl, 2 mM KCl, 1 mM $MgCl_2$, 0.6 mM $CaCl_2$, 10 mM HEPES, with or without 5 mM $NaH_2PO_4$, adjusted to pH 7.5 with Tris-base.

Before Pi influx measurement, the oocytes were transferred into Barth's solution containing 5 mM Pi with $^{33}$P (1 mCi ml$^{-1}$ $H_3{}^{33}PO_4$), incubated in buffer at either pH 5.5 or 7.5 for 2 h. After 2 h of incubation at 18 °C, the oocytes were washed with Barth's solution five times and then the radioactivity in the oocytes was measured.

*Transport activity of OsVPE2 is independent of G3P. YFP–OsVPE2* cRNA or water-injected oocytes were incubated in Barth's solution without Pi for 2 days at 18 °C. Oocytes were injected with 0 mM G3P or 5 mM G3P and transferred into Barth's solution (pH 5.5) containing 5 mM Pi with $^{33}$P (1 mCi ml$^{-1}$ $H_3{}^{33}PO_4$) for 2 h. After 2 h of incubation at 18 °C, the oocytes were washed with Barth's solution five times and then the radioactivity in the oocytes was measured.

*Anion selectivity of OsVPE2 in oocytes*. Oocytes expressing *OsVPE2* or water-injected negative control were exposed to $^{33}$P for 2 h at pH 5.5 in the external solution in the presence of 30 mM non-labelled Pi or 30 mM of other anions, including malate, nitrate, sulfate and chloride. After 2 h of incubation at 18 °C, the oocytes were washed with Barth's solution five times and then the radioactivity in the oocytes was measured.

**Patch-clamp recordings on isolated vacuoles.** Protoplasts of wild-type, double mutant and *OsVPE2* overexpression lines were isolated as described previously[34]. The vacuoles were isolated from protoplasts via a previously described procedure[37]. The ionic currents across the tonoplast were recorded using a standard patch-clamp procedure as previously described[9]. Recordings were performed using an Axon Axopatch 200B Amplifier (Molecular Devices). The pipette solution contained 100 mM $H_3PO_4$,1 mM $CaCl_2$, 2 mM $MgCl_2$ and 5 mM Mes-BTP (pH 5.8). The bath solution contained 100 mM $H_3PO_4$, 6.7 mM EGTA, 5.864 mM $CaCl_2$ and 5 mM Mes-BTP (pH 7.0). The osmolality of the pipette and bath solution was adjusted to 520 and 500 mosmol kg$^{-1}$, respectively, with D-sorbitol.

**Phylogenetic analysis.** The protein sequences of GlpT proteins from different species were retrieved from PLAZA (http://bioinformatics.psb.ugent.be/plaza/). The protein sequences of MpGlpT proteins were retrieved from phytozome (https://phytozome.jgi.doe.gov/). Phylogenetic analysis was conducted with CIPRES (www.phylo.org) using maximum-likelihood phylogenetic analysis with 1,000 bootstrap replicates. *C. reinhardtii* GlpT was used as an outgroup.

**Reporting Summary.** Further information on research design is available in the Nature Research Reporting Summary linked to this article.

## Data availability

The data that supports the findings of this study are available within the article and its Supplementary Information files or from the corresponding authors upon reasonable request.

Received: 11 July 2018; Accepted: 22 November 2018;
Published online: 9 January 2019

## References

1. Balzergue, C. et al. Low phosphate activates STOP1–ALMT1 to rapidly inhibit root cell elongation. *Nat. Commun.* **8**, 15300 (2017).
2. Muller, J. et al. Iron-dependent callose deposition adjusts root meristem maintenance to phosphate availability. *Dev. Cell* **33**, 216–230 (2015).
3. Kanno, S. et al. A novel role for the root cap in phosphate uptake and homeostasis. *eLife* **5**, e14577 (2016).
4. Raghothama, K. G. Phosphate acquisition. *Annu. Rev. Plant Physiol. Plant Mol. Biol.* **50**, 665–693 (1999).
5. Guo, B. et al. Functional analysis of the *Arabidopsis* PHT4 family of intracellular phosphate transporters. *New Phytol.* **177**, 889–898 (2008).
6. Versaw, W. K. & Harrison, M. J. A chloroplast phosphate transporter, PHT2;1, influences allocation of phosphate within the plant and phosphate-starvation responses. *Plant Cell* **14**, 1751–1766 (2002).
7. Picault, N., Hodges, M., Palmieri, L. & Palmieri, F. The growing family of mitochondrial carriers in *Arabidopsis*. *Trends Plant Sci.* **9**, 138–146 (2004).
8. Foyer, C. & Spencer, C. The relationship between phosphate status and photosynthesis in leaves: effects on intracellular orthophosphate distribution, photosynthesis and assimilate partitioning. *Planta* **167**, 369–375 (1986).
9. Liu, J. et al. A vacuolar phosphate transporter essential for phosphate homeostasis in *Arabidopsis*. *Proc. Natl Acad. Sci. USA* **112**, E6571–E6578 (2015).
10. Liu, T. Y. et al. Identification of plant vacuolar transporters mediating phosphate storage. *Nat. Commun.* **7**, 11095 (2016).
11. Wang, C. et al. Rice SPX-major facility superfamily 3, a vacuolar phosphate efflux transporter, is involved in maintaining phosphate homeostasis in rice. *Plant Physiol.* **169**, 2822–2831 (2015).
12. Elvin, C. M., Hardy, C. M. & Rosenberg, H. Pi exchange mediated by the GlpT-dependent *sn*-glycerol-3-phosphate transport system in *Escherichia coli*. *J. Bacteriol.* **161**, 1054–1058 (1985).
13. Huang, Y., Lemieux, M. J., Song, J., Auer, M. & Wang, D. N. Structure and mechanism of the glycerol-3-phosphate transporter from *Escherichia coli*. *Science* **301**, 616–620 (2003).
14. Ramaiah, M., Jain, A., Baldwin, J. C., Karthikeyan, A. S. & Raghothama, K. G. Characterization of the phosphate starvation-induced glycerol-3-phosphate permease gene family in *Arabidopsis*. *Plant Physiol.* **157**, 279–291 (2011).
15. Kawai, H. et al. *Arabidopsis* glycerol-3-phosphate permease 4 is localized in the plastids and involved in the accumulation of seed oil. *Plant Biotechnol.* **31**, 159–165 (2014).
16. Shen, J. et al. Organelle pH in the *Arabidopsis* endomembrane system. *Mol. Plant* **6**, 1419–1437 (2013).
17. Guo, M. et al. Integrative comparison of the role of the PHOSPHATE RESPONSE1 subfamily in phosphate signaling and homeostasis in rice. *Plant Physiol.* **168**, 1762–1776 (2015).
18. Popova, Y., Thayumanavan, P., Lonati, E., Agrochao, M. & Thevelein, J. M. Transport and signaling through the phosphate-binding site of the yeast Pho84 phosphate transceptor. *Proc. Natl Acad. Sci. USA* **107**, 2890–2895 (2010).
19. Law, C. J., Enkavi, G., Wang, D. N. & Tajkhorshid, E. Structural basis of substrate selectivity in the glycerol-3-phosphate: phosphate antiporter GlpT. *Biophys. J.* **97**, 1346–1353 (2009).
20. Ma, X. et al. A robust CRISPR/Cas9 system for convenient, high-efficiency multiplex genome editing in monocot and dicot plants. *Mol. Plant* **8**, 1274–1284 (2015).
21. Hou, X. L. et al. Regulation of the expression of *OsIPS1* and *OsIPS2* in rice via systemic and local Pi signalling and hormones. *Plant Cell Environ.* **28**, 353–364 (2005).
22. Ai, P. et al. Two rice phosphate transporters, OsPht1;2 and OsPht1;6, have different functions and kinetic properties in uptake and translocation. *Plant J.* **57**, 798–809 (2008).
23. Wang, C. et al. Involvement of OsSPX1 in phosphate homeostasis in rice. *Plant J.* **57**, 895–904 (2009).
24. Bustos, R. et al. A central regulatory system largely controls transcriptional activation and repression responses to phosphate starvation in *Arabidopsis*. *PLoS Genet.* **6**, e1001102 (2010).
25. Wang, X. et al. Trans-Golgi network-located AP1 gamma adaptins mediate dileucine motif-directed vacuolar targeting in *Arabidopsis*. *Plant Cell* **26**, 4102–4118 (2014).
26. Rausch, C. & Bucher, M. Molecular mechanisms of phosphate transport in plants. *Planta* **216**, 23–37 (2002).

27. Tohge, T. et al. Toward the storage metabolome: profiling the barley vacuole. *Plant Physiol.* **157**, 1469–1482 (2011).
28. Pant, B.-D. et al. Identification of primary and secondary metabolites with phosphorus status-dependent abundance in *Arabidopsis*, and of the transcription factor PHR1 as a major regulator of metabolic changes during phosphorus limitation. *Plant Cell Environ.* **38**, 172–187 (2015).
29. Moradi, M., Enkavi, G. & Tajkhorshid, E. Atomic-level characterization of transport cycle thermodynamics in the glycerol-3-phosphate:phosphate antiporter. *Nat. Commun.* **6**, 8393 (2015).
30. Wang, C. et al. Functional characterization of the rice SPX-MFS family reveals a key role of OsSPX-MFS1 in controlling phosphate homeostasis in leaves. *New Phytol.* **196**, 139–148 (2012).
31. Deng, M. et al. OsCYCP1;1, a PHO80 homologous protein, negatively regulates phosphate starvation signaling in the roots of rice (*Oryza sativa* L.). *Plant Mol. Biol.* **86**, 655–669 (2014).
32. Li, Y. et al. *Chalk5* encodes a vacuolar $H^+$-translocating pyrophosphatase influencing grain chalkiness in rice. *Nat. Genet.* **46**, 398–404 (2014).
33. Wu, F. H. et al. Tape-*Arabidopsis* Sandwich—a simpler *Arabidopsis* protoplast isolation method. *Plant Methods* **5**, 16 (2009).
34. Zhang, Y. et al. A highly efficient rice green tissue protoplast system for transient gene expression and studying light/chloroplast-related processes. *Plant Methods* **7**, 30 (2011).
35. Nelson, B. K., Cai, X. & Nebenfuhr, A. A multicolored set of in vivo organelle markers for co-localization studies in *Arabidopsis* and other plants. *Plant J.* **51**, 1126–1136 (2007).
36. Nour-Eldin, H. H., Hansen, B. G., Norholm, M. H., Jensen, J. K. & Halkier, B. A. Advancing uracil-excision based cloning towards an ideal technique for cloning PCR fragments. *Nucleic Acids Res.* **34**, e122 (2006).
37. De Angeli, A., Zhang, J., Meyer, S. & Martinoia, E. AtALMT9 is a malate-activated vacuolar chloride channel required for stomatal opening in *Arabidopsis*. *Nat. Commun.* **4**, 1804–1804 (2013).

## Acknowledgements

The authors thank B. Menand for valuable suggestions, J. M. Thevelein for the yeast strains, and L. Jiang and G. Miesenböck for the PEpHluorin and PRpHluorin. This work was supported by the National Key Research and Development Program of China (2017YFD0200204) and the National Natural Science Foundation (31772386, 31801924 and 31670267). K.Y. was supported by the National Program for the Support of Top-notch Young Professionals and the Innovation Program of Chinese Academy of Agricultural Sciences. L.D. is funded by a European Research Council Advanced Grant (EVO-500; contract number 25028). S.L. is funded by a grant from the National Science Foundation.

## Author contributions

K.Y. conceived and supervised the project. L.X., H.Z. and K.Y. designed the research. L.X., H.Z., R.W., Y.L., Z.X., W.T., W.R., F.W., M.D. and J.W. performed the experiments. L.X., H.Z., R.W., L.D., S.L., S.X. and K.Y. analysed the data. L.X., H.Z. and K.Y. wrote the paper with contributions from all the authors.

## Competing interests

The authors declare no competing interests.

## Additional information

**Supplementary information** is available for this paper at https://doi.org/10.1038/s41477-018-0334-3.

**Reprints and permissions information** is available at www.nature.com/reprints.

**Correspondence and requests for materials** should be addressed to K.Y.

**Publisher's note:** Springer Nature remains neutral with regard to jurisdictional claims in published maps and institutional affiliations.

nature research

Corresponding author(s): Keke Yi

# Reporting Summary

Nature Research wishes to improve the reproducibility of the work that we publish. This form provides structure for consistency and transparency in reporting. For further information on Nature Research policies, see Authors & Referees and the Editorial Policy Checklist.

## Statistical parameters

When statistical analyses are reported, confirm that the following items are present in the relevant location (e.g. figure legend, table legend, main text, or Methods section).

| n/a | Confirmed |
|---|---|
| ☐ | ☒ The exact sample size (*n*) for each experimental group/condition, given as a discrete number and unit of measurement |
| ☐ | ☒ An indication of whether measurements were taken from distinct samples or whether the same sample was measured repeatedly |
| ☐ | ☒ The statistical test(s) used AND whether they are one- or two-sided<br>*Only common tests should be described solely by name; describe more complex techniques in the Methods section.* |
| ☒ | ☐ A description of all covariates tested |
| ☒ | ☐ A description of any assumptions or corrections, such as tests of normality and adjustment for multiple comparisons |
| ☒ | ☐ A full description of the statistics including central tendency (e.g. means) or other basic estimates (e.g. regression coefficient) AND variation (e.g. standard deviation) or associated estimates of uncertainty (e.g. confidence intervals) |
| ☐ | ☒ For null hypothesis testing, the test statistic (e.g. *F*, *t*, *r*) with confidence intervals, effect sizes, degrees of freedom and *P* value noted<br>*Give P values as exact values whenever suitable.* |
| ☒ | ☐ For Bayesian analysis, information on the choice of priors and Markov chain Monte Carlo settings |
| ☒ | ☐ For hierarchical and complex designs, identification of the appropriate level for tests and full reporting of outcomes |
| ☒ | ☐ Estimates of effect sizes (e.g. Cohen's *d*, Pearson's *r*), indicating how they were calculated |
| ☐ | ☒ Clearly defined error bars<br>*State explicitly what error bars represent (e.g. SD, SE, CI)* |

*Our web collection on statistics for biologists may be useful.*

## Software and code

Policy information about availability of computer code

| | |
|---|---|
| Data collection | A Bruker AscendTM 600 spectrometer with TopSpin software version 3.0 was used to measure Pi concentration of vacuolar and cytoplasmic in rice root. |
| Data analysis | Student's t tests were conducted using Excel. The NMR data were analyzed using MestReNova 8.1.<br>The MS/MS data were processed using Mascot search engine (v.2.3.0).<br>Phylogenetic analysis was conducted with CIPRES Science Gateway V 3.3. |

For manuscripts utilizing custom algorithms or software that are central to the research but not yet described in published literature, software must be made available to editors/reviewers upon request. We strongly encourage code deposition in a community repository (e.g. GitHub). See the Nature Research guidelines for submitting code & software for further information.

## Data

Policy information about availability of data

All manuscripts must include a data availability statement. This statement should provide the following information, where applicable:

- Accession codes, unique identifiers, or web links for publicly available datasets
- A list of figures that have associated raw data
- A description of any restrictions on data availability

The data that supports the findings of this study are available within the article and its Supplementary Information files or from the corresponding author upon reasonable request.

# Field-specific reporting

Please select the best fit for your research. If you are not sure, read the appropriate sections before making your selection.

☒ Life sciences ☐ Behavioural & social sciences ☐ Ecological, evolutionary & environmental sciences

For a reference copy of the document with all sections, see nature.com/authors/policies/ReportingSummary-flat.pdf

# Life sciences study design

All studies must disclose on these points even when the disclosure is negative.

| | |
|---|---|
| Sample size | Sample sizes were chosen based on our experience on the experimental variability of this type of experiment and the desire to get statistically significant data to support meaningful conclusions.<br>Measurements of Pi concentration: two rice seedlings were collected for each biological replicate for each sample, in three biological replicates.<br>NMR analysis of Pi concentration of vacuolar and cytoplasmic: three rice seedlings were collected for each biological replicate for each sample, at least in three biological replicates.<br>Transport activity assay in xenopus laevis oocytes: eight biological replicates were performed.<br>Patch-Clamp recordings on Isolated vacuoles: more than ten vacuoles were collected for each sample.<br>Phenotyping: at least 4 plants for each genotype were used for comparing phenotypes between wild type and mutants. |
| Data exclusions | No data were excluded. |
| Replication | Every experiment was repeated for at least three times, and similar results were obtained. |
| Randomization | Sample allocation is not relevant to our study. Comparison of phenotypes was based on different genotypes. |
| Blinding | Experiments were not blinded. Data were always collected according to the genotype of plants. |

# Reporting for specific materials, systems and methods

### Materials & experimental systems

| n/a | Involved in the study |
|---|---|
| ☐ | ☒ Unique biological materials |
| ☒ | ☐ Antibodies |
| ☒ | ☐ Eukaryotic cell lines |
| ☒ | ☐ Palaeontology |
| ☒ | ☐ Animals and other organisms |
| ☒ | ☐ Human research participants |

### Methods

| n/a | Involved in the study |
|---|---|
| ☒ | ☐ ChIP-seq |
| ☒ | ☐ Flow cytometry |
| ☒ | ☐ MRI-based neuroimaging |

## Unique biological materials

Policy information about availability of materials

| | |
|---|---|
| Obtaining unique materials | Seeds of OsVPEs mutants, OsVPEs RNAi (Ri), OsVPEs overexpression, Osvpes complement lines , OsVPEs:GUS, 4xPIBS:GUS, Atglpt2-1, are available from the authors with no restrictions. |